Phys. Status Solidi A **208**, No. 9, 2093–2098 (2011) / **DOI** 10.1002/pssa.201100122

physica status solidi a
www.pss-a.com
applications and materials science

Real-time study of protein adsorption on thin nanocrystalline diamond

L. Grieten[*,1], S. D. Janssens[1], A. Ethirajan[1], N. Vanden Bon[2], M. Ameloot[2], L. Michiels[2], K. Haenen[1,3], and P. Wagner[1,3]

[1] Institute for Materials Research, Hasselt University, Wetenschapspark 1, 3590 Diepenbeek, Belgium
[2] Biomedical Research Institute, Hasselt University, Agoralaan, Bldg. C, 3590 Diepenbeek, Belgium
[3] IMEC vzw, Division IMOMEC, Wetenschapspark 1, 3590 Diepenbeek, Belgium

Received 1 May 2011, revised 13 July 2011, accepted 29 July 2011
Published online 1 September 2011

Keywords impedance spectroscopy, nanocrystalline diamond, protein adsorption

[*] Corresponding author: e-mail Lars.Grieten@uhasselt.be, Phone: +32-11-268817, Fax: +32-11-268899

The study of protein adsorption on solid surfaces is interesting for theoretical and practical bio-analytical sensing applications. In this work we combine electrochemical impedance spectroscopy, enzyme linked immunosorbent assay, and fluorescence microscopy with thin boron doped nanocrystalline diamond films to address and study the adsorption behavior of globular proteins (antibodies) on hydrophobic and hydrophilic diamond surfaces. A powerful combination of time resolved impedance spectroscopy and data modeling with equivalent circuits allow a detailed insight in the protein behavior at an interface. It is found that hydrogenated diamond is greatly favorable for impedimetric read-out but causes slight conformational loss of the protein structure and therefore also its biological activity. The oxidized surface allows faster adsorption and a high biological activity but results in smaller impedimetric response.

© 2011 WILEY-VCH Verlag GmbH & Co. KGaA, Weinheim

1 Introduction Boron-doped nanocrystalline diamond films (B-NCD) are ideal electrode material for electrochemical applications due to their extremely wide potential working ranges with negligibly small background current, various possibilities of surface functionalizations, biocompatibility, and stability in aqueous environments [1]. The unique physical and chemical properties of synthetic diamond are used in many scientific applications, ranging from corrosion resilient coatings [2] to electrochemistry [3–6] and biosensing [7–14]. Boron is the most common dopant used for obtaining semi-conductivity (10^{19} cm^{-3} to metallic diamond (10^{21} cm^{-3}) [15]. When boron doped diamond films are used in electrochemical applications for bio-analytical sensing, it is important to understand the interaction mechanisms of proteins with the interface. The physical adsorption of proteins at a liquid–solid interface is due to Van der Waals and ionic interactions. Therefore the study of protein adsorption onto solid surfaces is of practical importance in areas such as bio-analytical sensing [13], separation of biological solutions, and bio-compatibility of materials [16]. The adsorption of proteins on substrates often causes a loss of biological activity by partial unfolding or denaturation [17]. As mentioned before, the surface terminations of the diamond film can be tuned from hydrophilic (NCD:O) to hydrophobic (NCD:H) in order to tailor a suitable substrate for any kind of adsorption study or chemical modification of interest [9, 18–20]. Current techniques to study protein adsorption can be classified under optical techniques, such as optical waveguide light-mode spectroscopy, total internal reflection fluorescence, and ellipsometry and under non-optical techniques, such as the quartz crystal microbalance. Both techniques have advantages and drawbacks. The optical techniques show lack for precise kinetic adsorption data, the need for labeling with fluorescent dyes and transparent substrates. The non-optical techniques show sensitivity for viscous drag of the liquid contacting the surface and need piezoelectric properties of the transducer. In this paper, the semi conductive properties of B-NCD and electrochemical impedance spectroscopy (EIS) are combined in order to monitor molecular changes at the interface without the need for any visualization methods. In addition, the biological activity is tested with specialized enzyme linked immunosorbent assay (ELISA) protocols. Fluorescence measurements are used to confirm the results obtained with the impedimetric read-out.

© 2011 WILEY-VCH Verlag GmbH & Co. KGaA, Weinheim

2 Experimental

2.1 Materials Impedance measurements were conducted in homemade 1× phosphate buffered saline at pH 7.4 (10× PBS: 1.29 M NaCl, 0.05 M $Na_2HPO_4 \cdot 2H_2O$, 0.015 M KH_2PO_4). An ELISA amplification system based on the cyclic redox reaction of NADH/NAD+ was obtained from Invitrogen (Merelbeke, Belgium) for the biological activity specificity experiments. Unlabeled and alkaline phosphatase (AP)-labeled anti-CRP monoclonal antibodies, their specific antigen CRP were synthesized by Scipac (Kent, UK). Fluorescence measurements were done with a goat-anti mouse IgG labeled with an Alexa-488 fluorophore (Sigma Aldrich, Belgium).

2.2 Diamond synthesis Thin boron-doped nanocrystalline diamond films (B-NCD) were grown on highly conductive silicon substrates (1–20 Ω cm) by microwave plasma enhanced chemical vapour deposition (MWPECVD) using a 3% methane/hydrogen mixtures and 200 ppm trimethyl borane as dopant in an ASTeX reactor as described in Ref. [21]. The B-NCD samples served as the working electrode in a home-made set-up which allows impedimetric read-out. Hydrophobic diamond was prepared by hydrogenation in a H_2 plasma (50 Torr, 800 °C, power 4000 W, 14 min) [22]. The hydrophilic diamond was prepared by soaking the B-NCD films in a H_2SO_4/KNO_3 (2:1 wt%) mixture, heated to 250 °C for 10 min. Afterwards, the diamond was rinsed in DI water and dried under a flow of nitrogen. A final oxidation step was performed by placing the diamond film in a UV-OZONE system (Ames, Iowa) at 50 °C for 60 min.

2.3 Electrochemical impedance spectroscopy EIS was performed using a Hewlett Packard 4149A Impedance/Gain-Phase Analyzer (Agilent, Diegem, Belgium). The impedance was measured by applying a 50 mV AC voltage (U) in sweeps of 50 frequencies ranging from 100 Hz and 1 MHz. The response to this potential is an AC current signal (I). No DC-offset was used. Real-time impedance curves were recorded continuously and Nyquist plots were taken at specific timings. In order to stabilize the temperature, an incubator oven (Binder, Germany) is used at 37 °C. The electrochemical setup consists of a working electrode (NCD-film) and a platinum counter electrode. No reference electrode was used. After a stable impedance signal was obtained, 20 nM of antibodies (Sigma–Aldrich, Belgium) were added to the sensor cell in a constant flowrate of 250 μl/min. The total volume exchange took 1.5 min.

2.4 Fluoresence microscopy and ELISA Fluorescence measurements were made with a confocal microscope Zeiss LSM 510 META (Jena, Germany) equiped with a 30 mW argon ion laser. The Alexa fluorophores were excited by the 488 nm line of the ion laser. Emission light is passed through a 505 nm LP filter into a photomultiplier tube. All images were recorded at 10% of the acousto-optic tunable filter (AOTF) transmission (±33 μW at the sample position) to avoid bleaching. For the bleaching process, a rectangular region of interest (ROI) was defined. The bleaching was performed by applying 10 scans of the ROI with the AOTF transmission set to 100%. The recorded background was used to normalize the fluorescence results to quantify the intensity. ELISA was performed by a 15 min incubation of the primary antibody and a 2 h BSA blocking at room temperature. Further details about the experimental procedure are described in Ref. [14].

2.5 Modeling of the impedimetric results The time resolved impedance curves were modeled by a Boltzman fit in order to extract time constants of the adsorption process. Fitting the impedance data was done with ZsimpWin software (Princeton Applied Research, USA). The standardized equivalent circuit $R(QR)(QR)$ was used (Fig. 1). The fitted results are represented in Table 1. The equivalent model contains constant phase elements (CPE's) to obtain better fits. A CPE's impedance is defined as a complex number with Q representing a constant, ω the angular frequency and n a number between 1 (ideal capacitor) and 0 (pure resistor). A CPE is in fact a generalized imperfect capacitance that takes surface roughness and heterogeneities into account:

$$Z = \frac{1}{(Qi\omega)^n}. \tag{1}$$

To obtain a better insight in the capacitive changes, a pseudo capacitance can be calculated from the constant phase element (Eq. (2)).

$$C = Q_{dl}(Q_{dl}R_{dl})^{\frac{1-n}{n}}. \tag{2}$$

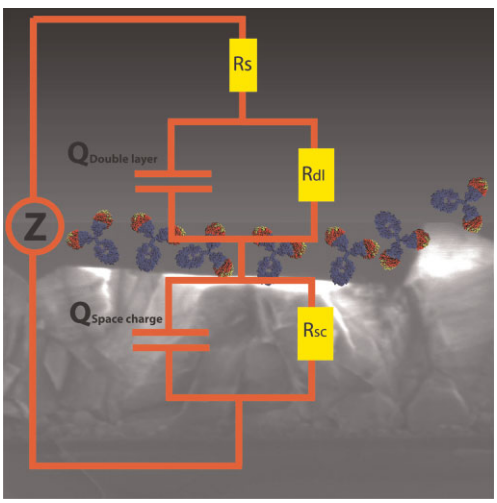

Figure 1 (online color at: www.pss-a.com) Schematic representation of a SEM cross-section of the diamond/protein interface and the corresponding equivalent models used to calculate the parameters of the impedance spectra. With R_s as the series resistance, Q_{dl}, R_{dl} the double layer capacitance and resistance. Q_{sc} and R_{sc} the space charge capacitance and resistance.The capacitors are treated as constant phase elements (Q).

© 2011 WILEY-VCH Verlag GmbH & Co. KGaA, Weinheim

Table 1 Fit results for the equivalent model for the oxidized (Ox-) and hydrogenated (H-) diamond samples. The components represent: the solution and electrode resistance (R_s), the double layer at the interface Q_{dl}, n_{dl}, and R_{dl} and the space charge region in the diamond film Q_{sc}, n_{sc}, and R_{sc}.

symbol	oxidized		hydrogenated		
	before ($t = 0$ min)	after ($t = 15$ min)	before ($t = 0$ min)	during ($t = 15$ min)	after ($t = 30$ min)
R_s (Ωcm)	80.36	79.96	77.77	79.21	79.15
Q_{sc} (S s^n/cm^2)	4.21×10^{-8}	4.31×10^{-8}	4.92×10^{-9}	3.92×10^{-9}	3.80×10^{-9}
n_{sc}	0.856	0.854	0.940	0.954	0.955
R_{sc} (Ωcm)	2771	2791	2430	2667	2794
Q_{dl} (S s^n/cm^2)	6.92×10^{-6}	6.60×10^{-6}	1.14×10^{-6}	1.01×10^{-6}	9.63×10^{-7}
n_{dl}	0.876	0.854	0.905	0.920	0.925
R_{dl} (Ωcm)	3.81×10^5	1.16×10^5	2.31×10^5	9.42×10^4	7.27×10^4
χ^2	1.19×10^{-4}	6.37×10^{-5}	1.19×10^{-4}	6.37×10^{-5}	5.94×10^{-5}

For further focus on the capacitance Eq. (2) can be expanded to Eq. (3):

$$C = \varepsilon_r \varepsilon_0 \frac{A}{d}. \tag{3}$$

In Eq. (3), ε_0 represents the vacuum permittivity, ε_r the relative permittivity of the material, A the surface area (m^2), and d the thickness of charge separation (m). When proteins are adsorbed at the diamond–liquid interface, the double layer thickness (d) increases, and causes the capacitance to decrease. In the equivalent model there are two capacitances. The first is a large double layer capacitance (μF) that originates from the liquid–diamond interface, *i.e.* the double layer at which the proteins will adsorb (Q_{dl}). The secondary capacitance originates from the diamond itself caused by the low doping profile, which creates a space charge region, giving rise to a relative smaller capacitance in the nF range (Q_{sc}). The interface capacitance is sensitive to physical changes, such as adsorption, whilst the space charge capacitance is more charge sensitive. The difference between these capacitances and the effect of proteins on these properties are in the scope of this article.

3 Results

3.1 Properties of the diamond film The thin nanocrystalline diamond film had a thickness of 150 nm with an average crystal size of 50 nm. The measured roughness (AFM) is 13.8 nm and the contact angles, measured with MilliQ, were $93 \pm 1^\circ$ in case of hydrogenated diamond while non-measurable for the oxidized diamond. Figure 2 shows a SEM recording of the diamond film which clearly shows the nanocrystals (left) and a fluorescence image with a bleach line of the adsorbed protein layer (right).

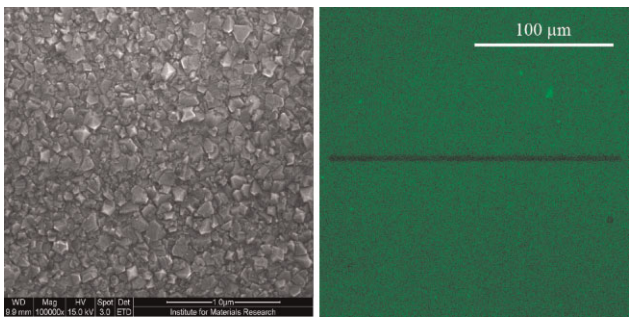

Figure 2 (online color at: www.pss-a.com) On the left, a SEM recording of the B-NCD sample with an average grain size of 50 nm is depicted. On the right, a confocal fluorescence image is shown with a rectangular bleach line to differentiate between the fluorophores and the background reflection.

3.2 Protein adsorption on oxidized and hydrogenated diamond films After a stabilized impedance signal was obtained in 1 × PBS buffer, antibodies were added with a flowrate of 250 µl/min (20 nM). After addition the system was switched to a stagnant (no flow) condition. By using time resolved impedance spectroscopy crucial information can be obtained about the protein adsorption processes. The change in impedance is proportional for the adsorbed proteins on the surface. During adsorption 2 different phases are observed. The first is the initial rate of adsorption (fast and linear) and after 50% of response (slower) kinetic effects start to dominate. The oxidized diamond reached saturation after 16 min (Fig. 3A) and this doubled in the case of hydrogenated diamond (Fig. 3B). Also the magnitude of impedimetric response is more than a tenfold lower for the oxidized diamond surface in comparison with the hydrogenated surface. Similar effects can be seen in the Nyquist plots. The R_{sc} of the H-diamond shows a supressed first semicircle in the initial state which drastically increases after adsorption until it reaches a maximum which is almost identical with the Ox-diamond after adsorption. The series resistance (R_s) shows no significant changes before and after adsorption in both cases. For the oxidized diamond the space charge capacitance is not influenced and will provide no further information about the adsorption process. The double layer capacitance (Ox-Q_{dl}) however

© 2011 WILEY-VCH Verlag GmbH & Co. KGaA, Weinheim

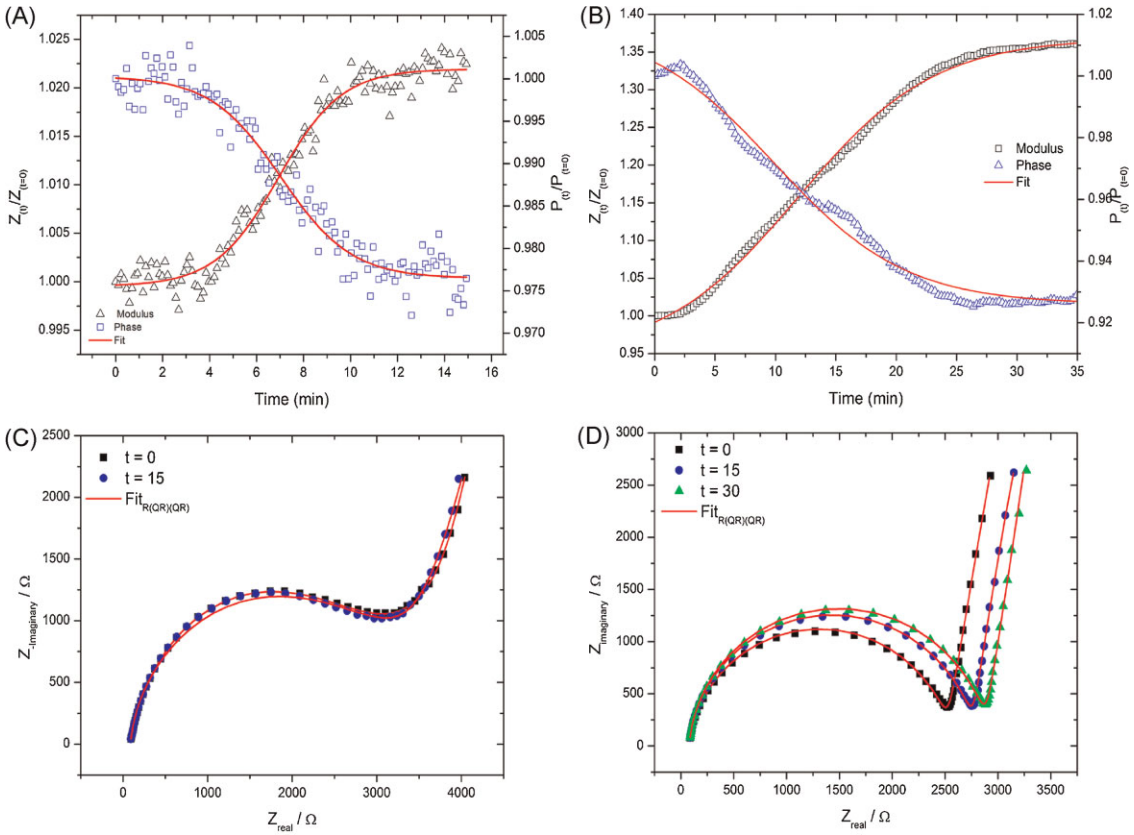

Figure 3 (online color at: www.pss-a.com) Time resolved impedance of the oxidized (A) and hydrogenated (B) diamond films and the corresponding Nyquist plots at specific timings with the equivalent fit for the oxidized (C) and the hydrogenated (D) diamond.

decreases indicating that interface changes are occurring. The hydrogenated diamond also exerts the same double layer changes. Additionally the space charge capacitance decreases significantly. Additional data obtained from an adapted ELISA show colorimetric results of the biological activity (Fig. 4B). A higher biological response of the adsorbed proteins on the oxidized diamond in comparison with the hydrogenated diamond is obtained. Confocal fluorescence microscopy provides qualitative information about the overall surface coverage. Here, proteins were adsorbed and washed at different time intervals, the fluorescence was measured in a liquid set-up and the results were normalized *versus* a bleach line (Fig. 4A). After 15 min there is almost a saturation of the fluorescence, only an insignificant increase is observed afterwards (30 min) in both the NCD:H and NCD:O.

4 Discussion Antibodies are globular proteins with a high water solubility. These proteins fold into organized, compact, and roughly spherical shapes in a way which allows hydrophobic amino acid side chains to localize on the inside of the sphere while the hydrophilic side chains are localized on the interface with the aqueous medium. The natural structure of proteins is dictated by their amino acid sequence, their interaction with solvent molecules, the pH, and the ionic composition of the solvent. Their quaternary structure tends to fold in such a way that they form the most stable, *i.e.*, lowest free energy structure. Also, this form is responsible for their biological activity. The ionic properties of proteins, determined primarily by their amino acid side chains, are pH dependent. The iso-electric point (IEP) is a pH value by which the net overall charge is zero. Antibodies have an IEP around pH 6 giving them a slight negative charge at pH 7.4. The presence of polar groups at the oxidized surface facilitates the adsorption of proteins, which have their hydrophilic groups located at the protein/water interface. The adsorption process can be monitored real-time and *in situ* by impedance spectroscopy. At different time intervals the complex plane plots are modeled with the equivalent circuit described in Fig. 1. Qualitative fits were obtained with χ^2 less than 10^{-4}. The selection of the appropriate model fulfilled the Boukamp theorem and is therefore the most relevant [23].

Oxidized diamond surfaces were prepared by UV–ozone treatment. Ozone is a very active molecule and is decomposed to form oxygen radicals. These attack the surface and exchanges the hydrogen for oxygen. This creates a polar character and causes a low water contact angle (5°). The time resolved impedance of the protein adsorption at 100 Hz (Fig. 3A) causes the modulus to slope upward and the phase to slope down to reach a saturation after 16 min. Nyquist plots before ($t = 0$ min) and after ($t = 15$ min) protein addition are represented in Fig. 3C. The modeled values

© 2011 WILEY-VCH Verlag GmbH & Co. KGaA, Weinheim

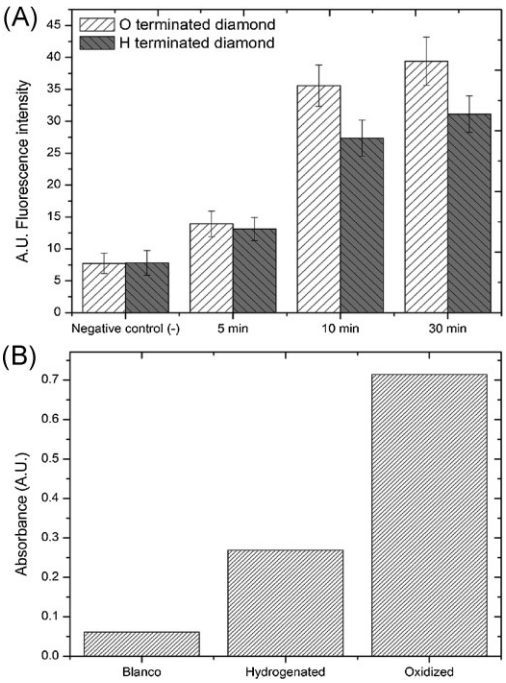

Figure 4 (A) Fluorescence results measured at 5, 10, and 30 min for the direct adsorption of the Ab-488 Alexa labelled antibody on oxidized and hydrogenated diamond. (B) ELISA results as biological assay with the immunogenic complex for the oxidized and hydrogenated diamond.

show a decrease in the double layer capacitance Q_{dl} caused by changes in the thickness (d) and relative permittivity (ε) after protein settling at the interface. The rest of the Nyquist spectrum shows no significant differences.

The real-time impedimetric response of the protein adsorption on the hydrogenated diamond surface at 100 Hz (Fig. 3B) shows a similar behavior as the oxidized surface. Remarkably the effect size is tenfold larger than the oxidized surface. Also the Nyquist plots (Fig. 3D) not only show shifts in the low frequencies, but also in the first hemisphere of the Nyquist. Once a globular protein (hydrophilic outer shell) adsorbs on a hydrophobic surface, a conformational change occurs. Therefore, creating a denser and more adhered layer causing an augmented effect on the double layer parameters. Interestingly the H-R_{dl} decreases after adsorption. This effect is also observed by Rezek *et al*. in which they state that proteins decrease the electrolyte electronic barrier induced by C–H dipoles and facilitate another route for charge transfer across the interface [24]. AFM studies from literature on protein conformation and thicknesses on diamond show a larger thickness on oxidized- in comparison with hydrogenated diamond [24, 25]. This is caused by the hydrophobic protein core that remains surrounded by hydrophilic parts upon adsorption on a hydrophilic surface. In our case the Q_{dl} decrease is much higher on NCD:O than on NCD:H diamond which indicates that the protein thickness is larger on NCD:O. Besides the Q_{dl} and R_{dl} an interesting parameter is the associated n value of the constant phase element. The fact that it reduces on oxidized- and increases on hydrogenated diamond suggests a different protein behavior at the surface. As mentioned before, proteins tend to exfoliate their hydrophobic inner part to a hydrophobic surface, therefore creating a tight packing and reducing the roughness. The reduction in roughness results in an increase in the H-n_{dl}. For the oxidized diamond surface the Ox-n_{dl} decreases because proteins are setteling without conformational changes. This is also confirmed in literature where a similar effect is found by AFM studies of protein adsorption on diamond [26] Besides the capacitive changes there is an additional effect. After plasma hydrogenation the diamond surface has C–H bonds creating positively charged dipoles that originate from electronegative differences. At the diamond–liquid interface there is a band bending profile (space charge region) due to the low doping of the diamond. The energy band of the H-terminated diamond surface moves upward to form an accumulation layer of holes near the surface. If negative charges are present at the surface, the energy band bending of the hydrogen termination can be enhanced and therefore causes the impedance to increase. This effect is also observed with DNA hybridization and denaturation [8, 27]. In addition to impedance spectroscopy, fluorescence is used as a qualitative tool to provide visual confirmation of the time resolved adsorption behavior between the oxidized- and hydrogenated diamond surfaces. After 15 min a saturation of adsorbed proteins is reached on both surfaces. However, the time and the impedimetric response for the hydrogenated diamond doubles and prolongs, respectively. Protein unfolding and rearrangement upon adsorption on the hydrophobic surface are responsible for this effect. The absolute difference between the hydrogenated and oxidized diamond at a single time interval could be due to quenching effects that occur on a hydrogenated diamond surface as described by Sakon *et al*. [28]. Figure 4B shows the ELISA results. This immunologic technique provides crucial information about the biological activity of the adsorbed proteins. A doubled biological activity for the NCD:O in comparison with the NCD:H was measured. The reduced signal for the hydrogenated diamond indicates that proteins partially lose their biological activity due to conformational changes when adsorbing on hydrophobic diamond and therefore confirm previous results. These results are also in good agreement with Hoffman *et al*. [17].

5 Conclusion The obtained results show that impedance spectroscopy is an interesting technique for the *in situ*, real-time study of protein adsorption. It withholds kinetic and protein behavioral information. By using hydrophobic or hydrophilic diamond it is possible to study the time resolved adsorption behavior of globular proteins. Hydrophilic diamond yields in a lower impedimetric response but results in a larger biological activity according to ELISA, because polar interactions between the protein and the interface do not promote conformational changes. Therefore it results in a faster adsorption rate. However the use of oxidized diamond

© 2011 WILEY-VCH Verlag GmbH & Co. KGaA, Weinheim

in impedance measurements requires low noise levels and stable conditions because only the interface properties change due to small capacitive effects. Hydrogenated diamond on the other hand is a favorable electrode material because it has a space charge sensitivity for the negative charged proteins. This results in a larger impedimetric response. A slight disadvantage is the partial loss of protein conformation. This yields in a tighter adsorbed layer on the interface which greatly influences the impedance and therefore causes an increased interface capacitance effect with additional space charge effects. The future use of hydrogenated diamond for protein sensor research is still important because the combination of impedance spectroscopy and nanocrystalline diamond withholds lot of benefits in comparison to other electrode materials. A question that rises with the obtained results is: Can hydrogenated diamond provide a sensitive surface for protein detection? Recently, an impedimetric protein sensor was developed with detection limits up to 10 nM on hydrogenated diamond [14]. Regardless of the loss in biofunctionality, the combination of the surface sensitivity of impedance spectroscopy with the high biological affinity of antibodies provides a promising combination for future protein research developments.

Acknowledgements In this work we gratefully acknowledge the support of Jan DHaen for the SEM recordings and Johnny Baccus for the technical support. Also the agency for Innovation by Science and technlogy (IWT). The research was performed in the framework of the IAP VI program Quantum Effects in Clusters and Nanowires, the Scientific Research Community WOG WO.035.04N Hybrid Systems at Nanometer Scale, the Fund for Scientific Research (FWO) projects G.082909 Synthetic diamond films as platform material for novel DNA sensors with electronic detection principles and G.0068.07 Growth, characterization and simulation of nanocrystalline and ultrananocrystalline PE-CVD diamond films, and the Methusalem project NANO Antwerp-Hasselt.

References

[1] C. Nebel, Thin-Film Diamond II, Vol. 77 (Academic Press, New York, 2004).
[2] S. Amirhaghi, H. S. Reehal, R. J. K. Wood, and D. W. Wheeler, Surf. Coat. Technol. **135**(2–3), 126–138 (2001).
[3] S. Ferro, M. Dal Colle, and A. De Battisti, Carbon **43**(6), 1191–1203 (2005).
[4] J. A. Garrido, S. Nowy, A. Haertl, and M. Stutzmann, Langmuir **24**(8), 3897–3904 (2008).
[5] N. G. Ferreira, L. L. G. Silva, E. J. Corat, and V. J. Trava-Airoldi, Diamond Relat. Mater. **11**(8), 1523–1531 (2002).
[6] T. N. Rao and A. Fujishima, Diamond Relat. Mater. **9**(3–6), 384–389 (2000).
[7] N. Bijnens, V. Vermeeren, M. Daenen, L. Grieten, K. Haenen, S. Wenmackers, O. Williams, M. Ameloot, M. vandeVen, L. Michiels, and P. Wagner, Phys. Status Solidi A **206**(3), 381 (2009).
[8] V. Vermeeren, N. Bijnens, S. Wenmackers, M. Daenen, K. Haenen, O. A. Williams, M. Ameloot, A. Vandeven, P. Wagner, and L. Michiels, Langmuir **23**(26), 13193–13202 (2007).
[9] A. Haertl, E. Schmich, J. Garrido, J. Hernando, S. C. R. Catharino, S. Walter, P. Feulner, A. Kromka, D. Steinmüller, and M. Stutzmann, Nature Mater. **3**(10), 736–742 (2004).
[10] A. Poghossian, M. H. Abouzar, A. Razavi, M. Backer, N. Bijnens, O. A. Williams, K. Haenen, W. Moritz, P. Wagner, and M. J. Schöning, Electrochim. Acta **54**(25), 5981–5985 (2009).
[11] M. H. Abouzar, A. Poghossian, A. Razavi, O. A. Williams, N. Bijnens, P. Wagner, and M. J. Schöning, Biosens. Bioelectron. **24**(5), 1298–1304 (2009).
[12] D. T. Tran, V. Vermeeren, L. Grieten, S. Wenmackers, P. Wagner, J. Pollet, K. P. P. Janssen, L. Michiels, and J. Lammertyn, Biosens. Bioelectron. **26**(6), 2987–2993 (2011).
[13] V. Vermeeren, S. Wenmackers, P. Wagner, and L. Michiels, Sensors **9**(7), 5600–5636 (2009).
[14] V. Vermeeren, L. Grieten, N. Vanden Bon, N. Bijnens, S. Wenmackers, S. D. Janssens, K. Haenen, P. Wagner, and L. Michiels, Sens. Actuators B **157**(1), 130–138 (2011).
[15] O. A. Williams, M. Daenen, J. D'Haen, K. Haenen, J. Maes, V. V. Moshchalkov, M. Nesladek, and D. M. Gruen, Diamond Relat. Mater. **15**(4–8), 654–658 (2006).
[16] Tang Liping, P. Thevenot, and Wenjing Hu, Curr. Top. Med. Chem. **8**, 270–280 (2008).
[17] R. Hoffmann, A. Kriele, S. Kopta, W. Smirnov, N. Yang, and C. Nebel, Phys. Status Solidi A **207**(9), 2073 (2010).
[18] P. Christiaens, V. Vermeeren, S. Wenmackers, M. Daenen, K. Haenen, M. Nesladek, M. vandeVen, M. Ameloot, L. Michiels, and P. Wagner, Biosens. Bioelectron. **22**(2), 2073–2077 (2006).
[19] N. Yang, J. Yu, H. Uetsuka, and C. E. Nebel, Electrochem. Commun. **11**(11), 2237–2240 (2009).
[20] J. Niedzialka-Jansson, S. Boland, R. Leech, D. Boukherroub, and S. Szunerits, Electrochim. Acta **55**(3), 959–964 (2010).
[21] O. A. Williams and M. Nesladek, Phys. Status Solidi A **203**(13), 3375 (2006).
[22] D. Y. Kim, J. Wang, J. Yang, H. W. Kim, and G. M. Swain, J. Phys. Chem. C **115**(20), (2011).
[23] M. Naumowicz, A. D. Petelska, and Z. A. Figaszewski, Electrochim. Acta **54**(3), 1089–1094 (2009).
[24] B. Rezek, M. Kratka, A. Kromka, and M. Kalbacova, Biosens. Bioelectron. **26**(4), 1307–1312 (2010).
[25] B. Rezek, L. Michalkov, E. Ukraintsev, A. Kromka, and M. Kalbacova, Sensors **9**(5), 3549–3562 (2009).
[26] B. Rezek, E. Ukraintsev, L. Michalkov, A. Kromka, J. Zemek, and M. Kalbacova, Diamond Relat. Mater. **18**(5–8), 918–922 (2009).
[27] B. van Grinsven, N. V. Bon, L. Grieten, M. Murib, S. D. Janssens, K. Haenen, E. Schneider, S. Ingebrandt, M. J. Schöning, V. Vermeeren, M. Ameloot, L. Michiels, R. Thoelen, W. De Ceuninck, and P. Wagner, Lab Chip **11**(9), (2011).
[28] J. J. Sakon, G. J. Ribeill, J. M. Garguilo, J. Perkins, K. R. Weninger, and R. J. Nemanich, Diamond Relat. Mater. **18**(1), 82 (2009).

© 2011 WILEY-VCH Verlag GmbH & Co. KGaA, Weinheim